Creep Behavior of a Large Full-Size Welded Austenitic Steel Plate

V. Koundy

L. Allais
CEA-CEREM,
Service de Recherches
Métallurgíques Appliquées,
CEA-Saclay,
91191 Gif-Sur-Yvette cedex, France

M. Delhaye
INSA-Rennes,
Département Génie Mécanique et
Automatique,
35043 Rennes cedex, France

The high-temperature design codes are presently considering the use of stress reduction factors for designing welded structures submitted to creep. These reduction factors are derived from creep tests which are generally made on small specimens and are not necessarily representative of large-size geometries. These codes are very likely overconservative, consequently uneconomical and need to be improved; an investigation to assess and quantify the supposed size effect is required. This paper presents an experimental and numerical study on creep behavior at 600°C of full-size welded joints taking into account real full-thickness of weldings. The material investigated is the austenitic stainless steel 316L(N) with manual metal arc welds using the 19 Cr 12 Ni 2 Mo electrode grade. The creep laws used in calculations are those obtained from tests using small specimens, but some coefficients of their theoretical formulation have been modified to obtain a better coherence with full-size specimen data. Between small and large full-size specimens, experimental results show no significant difference in time to rupture, and the same location of fracture, at the center of the weldment, is observed. Finite element simulations performed for full-size welded joints provide rupture times that are consistent with measured values. The calculated percentage of the damaged volume in the weld metal as a function of load levels and of creep-time duration is studied; it shows that the creep-rupture times for high stress loading are determined with higher accuracy than for low stress loading.

1 Introduction

Nuclear components in high-temperature plants, such as pressure vessels or sodium circuits in fast breeder reactors, are often designed to operate in the creep range. A very high level of life assurance of these components is required since their service life is long (30–40 y). They usually contain welded joints and the overall structural creep behavior of these welded joints is in most cases of a complex nature. In many situations, creep deterioration of weldment during high-temperature operation is responsible for failure in elevated temperature components. Additionally, laboratory creep rupture experiments show that creep damage first occurs in or in the vicinity of the welds when the predicted stress level in the weld region is about the same as that in the base metal.

A welded joint typically consists of three constituents: weld metal, heat-affected zone (HAZ) and base metal. When this joint is subjected to creep loading, each constituent shows a different creep characteristic. With regard to the welding process, weld deposits for austenitic stainless steel welds are required to have a minimum ferrite content to avoid hot cracking during welding. In addition, for components which are exposed for long times at elevated temperatures, an upper limit is imposed to the amount of ferrite in weld since ferrite undergoes transformation to brittle phases, such as sigma phase, during aging. Such phases are detrimental for the toughness evolution of the weld metal during service and for the creep ductility. On top of this, some chemical or residual elements (e.g., carbon, molybdenum, nitrogen, boron, phosphorus) are known to affect the elevated temperature strength and ductility of austenitic weld metals (Lundqvist and Anderson, 1982; Klueh and Edmonds, 1986; or Ohrt and te Heesen, 1991). These geometric, material and metallurgical discontinuities at welded joints thus complicate the evaluation of the component long-term structural integrity.

Currently, in the different design codes applicable to elevated temperature nuclear components such as the ASME Boiler and Pressure Vessel Code Case N-47 (1989) or the French code RCC-MR (1993), the creep-related design rules take account of the welded joints through a creep strength reduction factor which is primarily based on the stress rupture properties. These factors have been introduced for different types of welded joints on the basis of the analysis of the stress-to-rupture response of different weld metals. They relate the mean stress-to-rupture of each weld metal to the mean stress-to-rupture of the base materials, and are tabulated for different temperatures and times for several types of austenitic welds. Some of the background, logic and experimental validation of the factors used in the Code Case N-47 were provided by Corum (1990). In his work, a series of creep rupture tests carried out on simple welded plate and tubular structures fabricated from 316 stainless steel welded with 16-8-2 filler metal were also presented; the results tended to substantiate the validity of the strength reduction factor approach. Some designers, for example, Samuelson et al. (1992), stated that this approach, using a stress reduction to account for weldments, do not adequately account for the effect of the weldments on the load carrying capacity of the structure in the creep range. They suggested that an improved design methodology is one where the influence of the creep properties of the weld and HAZ materials, the geometry of the weld preparation and the loading conditions are considered.

Other works on the creep properties of austenitic welds are also relevant here. In the majority of cases the reported results have been obtained using standard size creep specimens (diameters 4 to 8 mm) and describe mainly the creep properties of different weld metals. Furthermore, Wood (1985) and Mathew et al. (1993) have given evidence that the rupture properties of many grades of welds are inferior to those of the corresponding

Contributed by the Pressure Vessels and Piping Division for publication in the JOURNAL OF PRESSURE VESSEL TECHNOLOGY. Manuscript received by the PVP Division, November 11, 1997; revised manuscript received February 26, 1998. Associate Technical Editor: S. K. Bhandari.

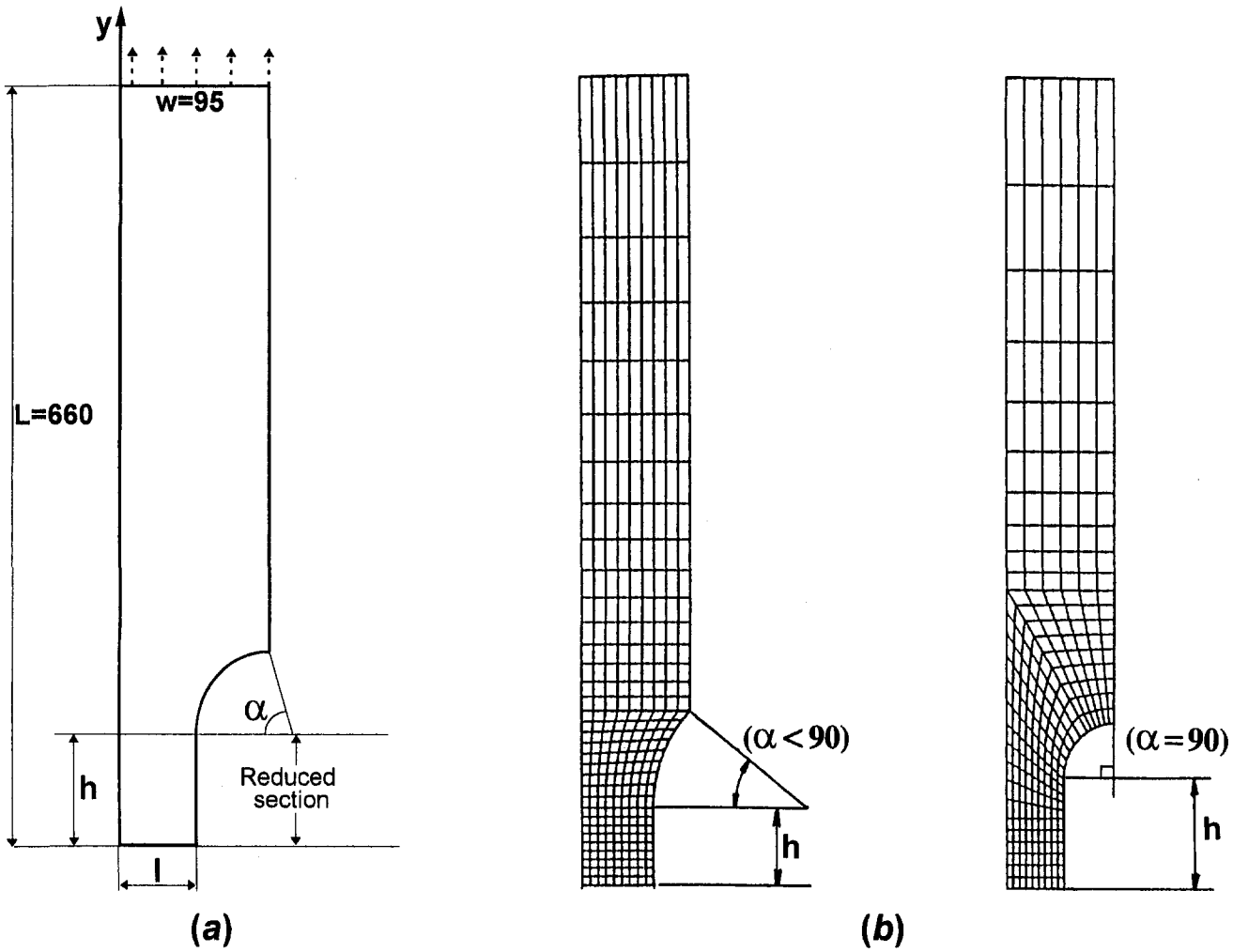

Fig. 1 A quarter of the specimen geometry—(*a*) dimensions (millimeters), (*b*) plane-stress finite element models

base material. Senior (1990), Smith and Farrar (1993) also showed that manual metal arc deposits of nominally the same composition can exhibit very large differences in creep properties.

These aforementioned results were acquired by using small test specimens and the influence of specimen geometry on creep test results for welded joints are not discussed. Some designers claim that geometry size effect on the results could be significant. Using finite element techniques, to predict creep behavior of welded joints in AISI 316 at a temperature of 600°C, Roode et al. (1980) showed that, for the same axial stress, the value of equivalent stress is lower in the large thick plate than in the standard size creep specimen machined across the weld. They also demonstrated that the axial creep strain in the weld metal is higher than that in the base metal, and this is different from the creep strain distribution in the standard test specimen. Similar work, concerning the creep behavior of welded joint of 304 stainless steel at a temperature of 550°C, was performed by Yamazaki et al. (1991). They established that the fracture took place in the base metal for small specimens, whereas it occurred at the weld metal for the large specimens. They also indicated that the change in location of fracture for small or large joint specimens was attributed to the plastic constraint at the base metal. Another interesting experimental and numerical study was presented by Dhalla (1991). He tested a full-scale 304 stainless steel intermediate heat exchanger at a temperature of 593°C and used finite element calculations taking into account one of the nozzles welded to the main cylinder. He observed creep rupture cracks in the weldments and revealed that the role of the residual stresses on creep rupture cracking is of secondary importance, and need not be numerically simulated in the elevated temperature design of weldments.

Faced with the lack of data on the practical behavior of large full-size (full-thickness) weld joints, a European program has been undertaken (CEC-BRITE-P2147, 1994). In this program, the experimental creep behavior of small and large specimens taken from the same welded joint was evaluated. Constitutive equations were derived for the parent and weld metals and these were applied in finite element analyses to predict the behavior of the large full-size specimens. The present investigation is realized as part of this European contract. The creep behavior at 600°C of a large full-size manual metal arc-welded plate has been treated experimentally and numerically. The aim is to assess and quantify the supposed "size" effect and also to determine whether the design codes are not too pessimistic by neglecting the constraint effect existing for small weld thicknesses and large plate thicknesses. Creep tests on full-size specimens may give accurate results for base metal and for weld joint.

This paper is divided into two sections. In the first section, the optimal geometric design of the specimen, the test conditions and the determination of the creep law used are presented. The second section contains the finite element simulations and the comparison between numerical and experimental results.

Table 1 Comparison of numerical results for different geometries

Loading	Results	Case 1	Case 2	Case 3	Case 4	Case 5
σ_y = 240 MPa	u_y (mm)	15.09	9.44	13.66	9.56	17.04
	$\Delta\sigma_{yy}$ (MPa) [a]	16	4	27	1	0
	$\frac{\sigma_{VM}^{max}}{\sigma_y}$ [b]	1.15	1.12	1.38	1.25	1.35
σ_y = 300 MPa	$\Delta\sigma_{yy}$ (MPa)	-	6	-	5	-
	$\frac{\sigma_{VM}^{max}}{\sigma_y}$	-	1.14	-	1.25	-
Extrapolation	$2u_y^f$ (mm)	247	192	230	195	250

[a] $\Delta\sigma_{yy}$ = axial stress gradient in the reduced section

[b] σ_{VM}^{max} = maximum value of the Von Mises equivalent stress

2 Specimen Optimal Geometric Design

The creep rupture tests were carried out at a temperature of 600°C and conducted on a heavy loading 250 tons hydraulic machine equipped with a thermal furnace. The 316L(N) austenitic stainless steel plate used for the specimen fabrication is rectangular, with a length of 1320 mm, a width of 190 mm, and a thickness of 25 mm. To perform creep tests up to rupture with an as-large size dimension specimen, a study to define and optimize its reduced section, using parametric elastoplastic calculations, was necessary. The main objectives of these calculations are:

- to obtain a final total elongation lower than the maximal displacement (200 mm) of the actuator-test apparatus,
- to achieve an axial stress in the active part of the specimen as homogeneous as possible,
- to minimize the maximum von Mises stress intensity.

For these preliminary calculations, the specimen was assumed to have no joint and to be at a homogeneous temperature of 600°C. Five finite element elastoplastic calculations were performed on five different geometries, as defined by (see Fig. 1(*a*)):

case 1: α = 45 deg l = 62.5 mm h = 62.5 mm (h/l = 1)
case 2: α = 60 deg l = 50 mm h = 75 mm (h/l = 1.5)
case 3: α = 90 deg l = 62.5 mm h = 62.5 mm (h/l = 1)
case 4: α = 90 deg l = 50 mm h = 88 mm (h/l = 1.76)
case 5: α = 90 deg l = 62.5 mm h = 125 mm (h/l = 2)

Given the symmetries, only a quarter of the specimen was modeled. Two types of the mesh, using eight-node plane-stress elements, were realized (Fig. 1(*b*)). The material characteristics are given by the RCC-MR code. Young's modulus and Poisson's ratio are, respectively, equal to E = 145,000 MPa and ν = 0.3. The stress-strain curve is that identified by Piques and Pineau (1984) and can be defined here by its best-fit function $\sigma = k\epsilon_p^n + R_{p02}$, with k = 1246, n = 0.807 and R_{p02} = 122 MPa; R_{p02} indicates the yield stress determined for a plastic deformation of 0.2 percent. The loading consists of a specimen tension with axial stress in the reduced section increasing up to 300 MPa. This maximum stress level is necessary to limit creep-rupture times to between 1000 and 3000 h. The calculations were performed with the general finite element INCA (1986) code. From elastoplastic calculation results, the final total elongation was estimated by a simple extrapolation method. This method considers an equivalent geometry of the half-specimen, composed of two bars connected in series. These bars, with lengths of ($L = x$) and x, represent the current part and the useful part (reduced section) of the equivalent structure, respectively. Their corresponding elastoplastic deformations ϵ_{Lx} and ϵ_x, assumed to be constant in each bar, are these determined by the elastoplastic calculation at the top and at the center of the specimen, respectively. Using the definition of the deformation $\epsilon = Ln((L + u_y)/L)$, with u_y the elastoplastic elongation, x can be determined by the following expression:

$$x = \frac{L(1 - \exp(\epsilon_{Lx})) + u_y}{\exp(\epsilon_x) - \exp(\epsilon_{Lx})} \tag{1}$$

In this method, the value of x, determined from the elastoplastic calculation results (ϵ_x, ϵ_{Lx}, and u_y) is supposed to remain constant. The final total elongation is then calculated by the following formula:

$$u_y^f = \underbrace{(L - x)(\epsilon_{l\max} + \epsilon_c)}_{\text{total elongation of current part}} + \underbrace{0.63x}_{\text{total elongation to rupture of useful part}} \tag{2}$$

where $\epsilon_{l\max}$ is the elastoplastic deformation at the end of loading, ϵ_c is the creep deformation supplied by the RCC-MR code, and the coefficient 0.63 denotes the total deformation at rupture of the useful part (63 percent represents the maximum value of the material ductility at rupture at 600°C). Table 1 gives the calculated results for two values of loading, 240 and 300 MPa. In all cases, the von Mises equivalent stress and the axial stress are almost identical; their maximum value is observed in the fillet (interface between the current part and the useful part). It

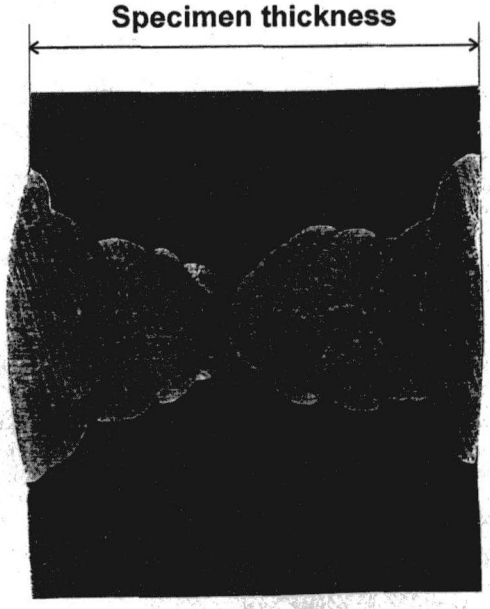

Fig. 2 Deposited weldment

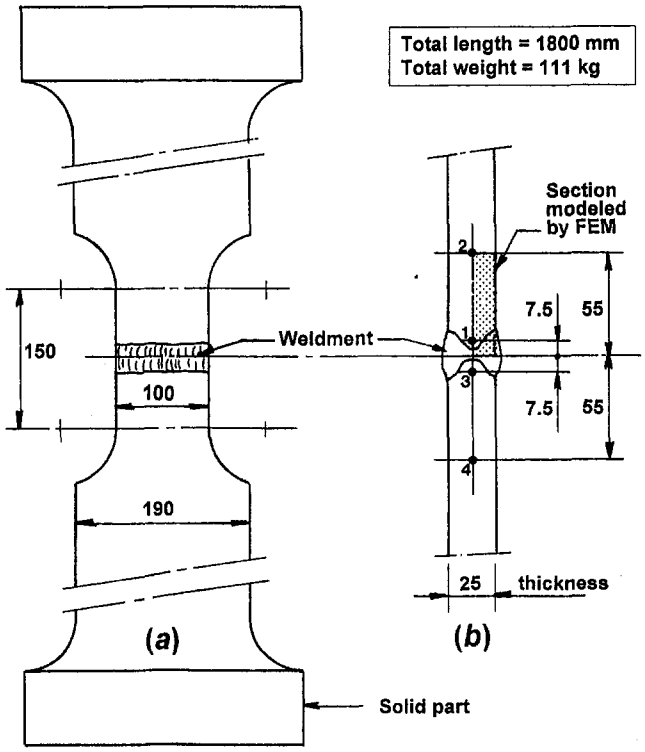

Fig. 3 Geometry of the large full-size specimen—(*a*) dimensions in millimeters; (*b*) general view of the four extensometer setting points

is shown that, among the five studied cases, the best compromise determined by this method is the geometry of case 2 with α = 60 deg. For this latter, the stress gradient in the reduced section as well as the local amplification of the von Mises equivalent stress is extremely low, and the final elongation (more pessimistic than the reality) is the lowest and corresponds to the maximum stroke permitted by the test apparatus (200 mm). Finally, this geometry (case 2) was adopted for the fabrication of the large full-size plate specimens.

3 Experimental Program

In this investigation, due to the complex experimental implementation, only two full-size weld joint creep tests at 600°C were performed under two stress levels, 240 and 265 MPa. In order to evaluate the creep performance of the full-size joint from experimental and computational points of view, more experimental data were required; creep properties of the base and weld metals, obtained by using conventional small specimens, were then used at the same time. These results from small specimens were provided by the RCC-MR code, by Escaravage et al. (1993), and also from our own available laboratory data. The latter results were augmented by those obtained from our own additional tests which were carried out at 600°C and under load stresses of 240 and 265 MPa, as described in the forthcoming.

3.1 Full-Size Welded Specimens The material investigated for the specimen welded joint fabrication is the austenitic stainless steel 316L(N) with two kinds of X-butt weld: manual metal arc (MMA) and tungsten inert gas (TIG) welds. For this study, only the MMA weld is considered and the electrode used for welding is of grade 19 Cr 12 Ni 2 Mo. The MMA X-shaped welded joint, in the middle of the reduced section, is composed in an upward vertical position with 7 runs on each side (see Fig. 2). All the chemical compositions and mechanical properties meet the requirements of the RCC-MR code.

The ends of the specimens were also welded together with two metallic solid parts required by the tensile testing machine system, as shown in Fig. 3(*a*). Two different extensometer systems were used; the first was mounted outside the furnace and measured the total elongation of the specimen on a 110-mm gage length and the second, working at elevated temperature, was utilized for weld metal strain measurements on a 15-mm basis. They were in contact with the specimen by four setting points as presented in Fig. 3(*b*). The regulated temperature along the gage length was controlled to within ±3°C. More details about experiments (welding parameters, chemical compositions, mechanical properties, test procedures) were presented by Allais et al. (1998). They studied the creep behavior of defect-free full-size weld joints and considered the two kinds of welds (MMA and TIG).

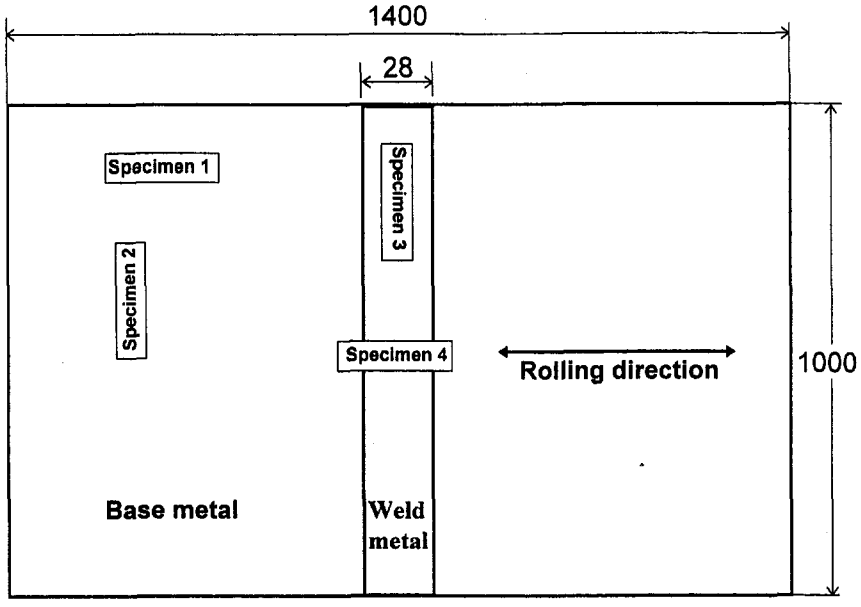

Fig. 4 Position and orientation of specimens inside the welded plate (dimensions in millimeters)

Table 2 Some creep law characteristics for the weld and base metals

Loading	Material	End of primary creep		Secondary creep rate	Creep strain (%)
		Time (h)	Strain (%)	(10^{-6} h^{-1})	at 1000 h
σ_y = 240 MPa	Weld metal	49	0.15	5.34	0.7
	Base metal	70	1.02	74.7	7.9
σ_y = 265 MPa	Weld metal	11	0.25	38.3	4.0
	Base metal	34	1.11	168.4	17.4

These experiments provide three types of results: the creep strain-time characteristics obtained with the aid of the extensometers, the times to rupture and the material rupture facies.

3.2 Conventional Small Specimens To determine the creep properties of the base and weld metals, six constant load creep rupture tests were carried out at 600°C—four under a load stress of 265 MPa and two under 240 MPa—on standard specimens. These small-size specimens, with a length of 20 mm and a diameter of 4 mm, were machined; their position and orientation inside the MMA-welded plate is shown in Fig. 4. Specimens 1 and 2 were taken from the base metal in the longitudinal and transversal directions, respectively. Specimen 3 was cut twice from the weld metal and specimen 4 machined twice across the weld.

3.3 Creep Laws Used for the Full-Size Specimen The characteristics of the used base metal are in agreement with those specified by the RCC-MR code. Nevertheless, the constitutive creep law, elaborated from small standard specimens and proposed by this code, had to be validated for our metal sheet. The primary and secondary stages of creep behavior are defined by Eqs. (3) and (4), respectively,

$$\epsilon = C_1 t^{C_2} \sigma^{n_1} \tag{3}$$

$$\dot{\epsilon} = C\sigma^n \tag{4}$$

where C_1, C_2, n_1, C and n are the material coefficients; the creep strain is expressed in percent. No attempt is made by this code to model the strain during the tertiary creep stage. The values of these coefficients given by the RCC-MR code, C_1 = 1.0225 10^{-12}, C_2 = 0.5134, n_1 = 4.6424, C = 2.268 10^{-24}, and n = 8.2, described correctly our experimental creep strain-time characteristics obtained from our small specimen tests (specimens 1 and 2 of Fig. 4) as well as from our full-size specimen tests. Stating that, for the last data related to the weld joint, the elongation of the base metal was determined from the global elongation defined by the following mixture law:

$$\epsilon_{\text{global}} = C_{\text{weld}}\epsilon_{\text{weld}} + C_{\text{base metal}}\epsilon_{\text{base metal}} \tag{5}$$

where C_{weld} and $C_{\text{base metal}}$ are the ratio of the length of the weld and base metals to the total specimen length, respectively.

Concerning the weld metal, the constitutive creep law presented by Escaravage et al. (1993) was considered. The same form of equation as that defined by Eqs. (3) and (4) was utilized. A comparison between their creep strain-time curves with those obtained on one hand from our small specimen tests (specimens 3 and 4 of Fig. 4), and on the other hand from our full-size specimen tests, showed that our experimental curves concerning 265 MPa were in agreement with their curves of 240 MPa. To suppress this gap, it was sufficient to correct their coefficients with the ratio of the two considered stress values (240/265). Hence, the new adopted coefficient values are: C_1 = 1.12 10^{-19}, C_2 = 0.17, n_1 = 7.5, C = 2.427 10^{-53}, and n = 19.89.

Some characteristics of these creep laws, related to the weld and base metals, are presented in Table 2. It is shown that the creep strain of the weld metal is clearly less than that displayed by the base metal.

4 Finite Element Simulation

The full-size specimen creep tests are modelized with the general finite element CASTEM 2000 code (1995). Eight-node plane-strain elements are used with an updated Lagrangian large displacement formulation. Due to the symmetries, it is only necessary to consider a quarter of the specimen thickness geometry (see Fig. 3(*b*)). Two models are made up of 2723 nodes and 868 elements, and of 2628 nodes and 837 elements, respectively; the meshes are presented in Fig. 5. The second model is used to study the effect of the real boundary shape of the weldment on the numerical results (see Fig. 2).

4.1 Elastoplastic and Creep Calculations Creep calculations were performed for two constant stress loadings, 240 and 265 MPa, with a temperature condition of 600°C. To reach these stress loading values, elastoplastic calculations were carried out. The stress-strain curve, related to the weld metal, is identified by our own tensile tests and can be defined by its best-fit function $\sigma = k\epsilon_p^n + R_{p02}$, with k = 619, n = 0.494 and R_{p02} = 225 MPa. It can be noted here that the yield stress R_{p02} (determined for a plastic deformation of 0.2 percent) is distinctly higher than that of the base metal which was given earlier.

4.2 Creep-Rupture Times Creep-rupture damage is calculated by using the following integral form, similar to that used in the RCC-MR or ASME-N47 code:

$$W = \int_0^T \frac{dt}{T_D(t)} \tag{6}$$

where T is the creep-time duration, and T_D denotes the allowable time at a given effective stress from loading. T_D values are obtained by entering in the stress-to-rupture curve a stress value equal to the calculated stress. The stress-to-rupture curve used, concerning the weld metal, is established from our experimental results obtained with small and large specimens as described previously. The best-fit function of these data, utilizing the same slope as that of the best-fit curve proposed by Escaravage et al. (1993), is presented in Fig. 6. In the creep finite element calculations, the Von Mises equivalent stress is given for each mesh point (or element) and for each time increment; by using the stress-to-rupture curve, we can deduct then the correspond-

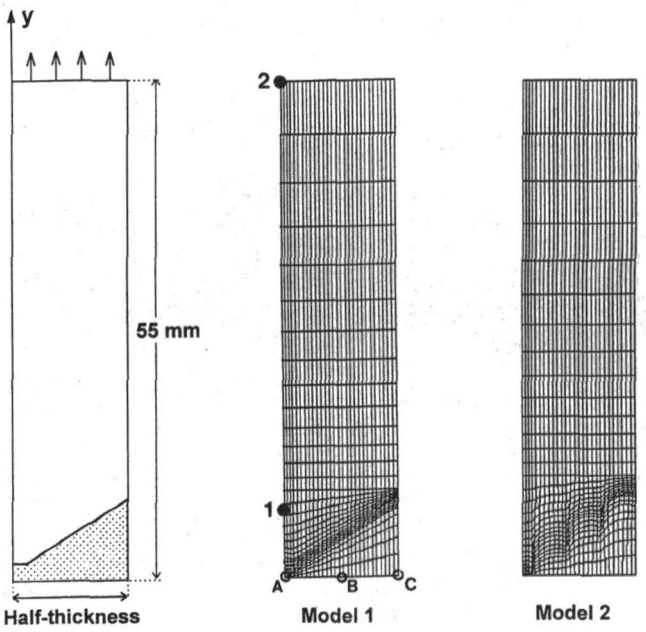

Fig. 5 Dimensions and meshes

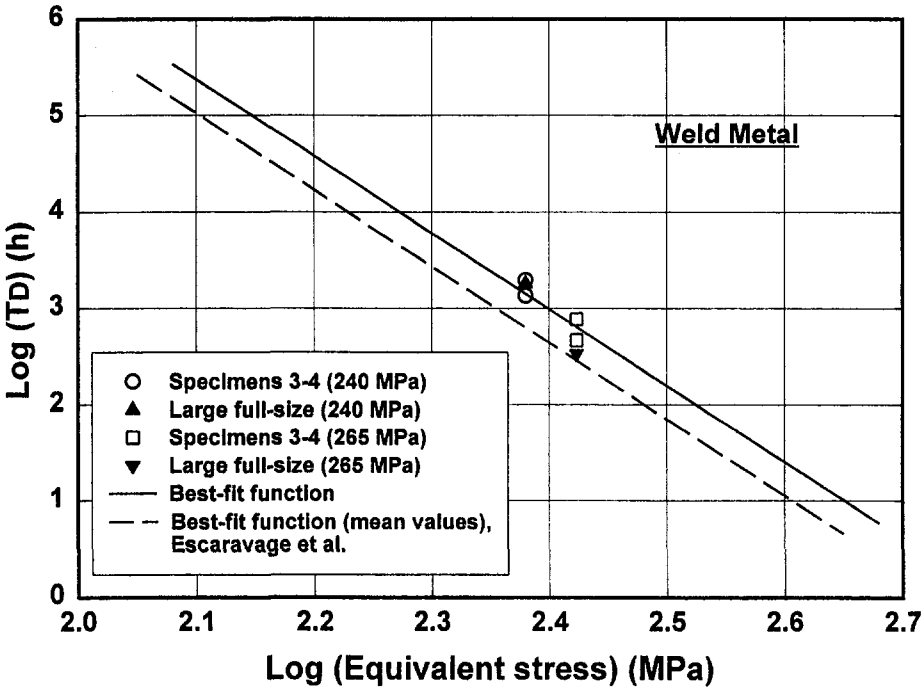

Fig. 6 Stress-to-rupture curves

ing value of T_D or a time-dependent function $T_D(t)$. The creep-rupture time is obtained when the value of the creep-rupture damage W is equal to 1. Thus, the creep-rupture time of the structure corresponds to the damage of the first element of the mesh.

5 Results and Discussion

Table 3 compares the calculated and experimental axial strains, at the end of the elastoplastic loading and at the extensometer setting points (Points 1 and 2 in Fig. 3(*b*) or Fig. 5). It can be seen that the calculated results are in good agreement with the experimental results.

Maximum stresses are localized in the weld metal; their values as function of time, for the constant stress loading 240 MPa, along the half-thickness (Points A, B, and C in Fig. 5), are presented in Table 4. It is shown that the maximum values of the Von Mises and principal stresses are located at the center (Point A) and at the edge (Point C) of the weld, respectively. It has been specified that Point A also corresponds to the location of the fracture initiation which was observed in our experiments, equally for the large full-size as well as small-size specimens. The calculated Von Mises equivalent stresses, capable of estimating the fracture location in the weldment, are therefore chosen for the time-dependent function $T_D(t)$ calculation (see Eq. (6)). It can be seen also in Table 4 that the stress redistribution takes place very rapidly (important stress variation at 1 h and low stress variation thereafter). Stress values are distinctly smaller in the base metal and their distribution is more homogeneous than in the weld metal. These comments are also true in the case of the constant stress loading 265 MPa.

Table 3 Axial elastoplastic strains at the extensometer setting points

At the end of elastoplastic loading	240 MPa		265 MPa	
	Weld metal (Point 1)	Base metal (Point 2)	Weld metal (Point 1)	Base metal (Point 2)
Experimental ε_y (%)	1.01	2.95	2.33	6.87
Calculated ε_y (%)	1.42	3.21	2.42	4.41

Table 4 Stresses as function of time along the half-thickness, under 240 MPa

Time	Stresses (MPa)	(Point A)	(Point B)	(Point C)
End of elastoplastic calculation	Von Mises	324	228	308
	Max. principal stress	120	215	340
1 h	Von Mises	262	230	258
	Max. principal stress	190	243	294
600 h	Von Mises	260	238	257
	Max. principal stress	191	251	289

Figure 7 illustrates the comparison between the calculated and measured creep strains at Point 1 (weld metal) for the two values of loading 240 and 265 MPa. In the case of 240 MPa (Fig. 7(*a*)), it can be seen that the calculated creep strains are clearly higher than the measured values; however, with the same form of curve, a small disparity is obtained between these two results. In the case of 265 MPa (Fig. 7(*b*)), a good agreement between the calculated and experimental creep strains is obtained for a creep duration of less than 100 h; after this time, an increasing divergence occurs, which is due to the tertiary creep observed during the experiment, and as already stated, is not taken into consideration in the numerical model.

Table 5 gives the comparison of the creep-rupture times for the two constant stress loadings 240 and 265 MPa, obtained by the experiments using small and large specimens as well as determined by calculations. In the latter results, two models were used (see Fig. 5) to study the effect on the rupture times when the boundary shape of the weldment approaches the reality. This table exhibits a fairly good accord with no significant difference in experimental time to rupture. It can be seen that the latter data are correctly estimated by the numerical models. The difference between the calculated rupture times and the measured values is visibly higher in the case of 240 MPa; however, this is a satisfactory result respecting that, on the one hand, the calculated rupture times here correspond only to the onset of the calculated damage in the weld metal and, on the other hand, it is well known that the scatter concerning experimental rupture times is significant in creep tests. Model 2, in which the interface boundary between the weld and base metals is better taken into account, improves the numerical results.

Figure 8 illustrates the percentage of the damaged volume in the weldment for various stress loads and as a function of the

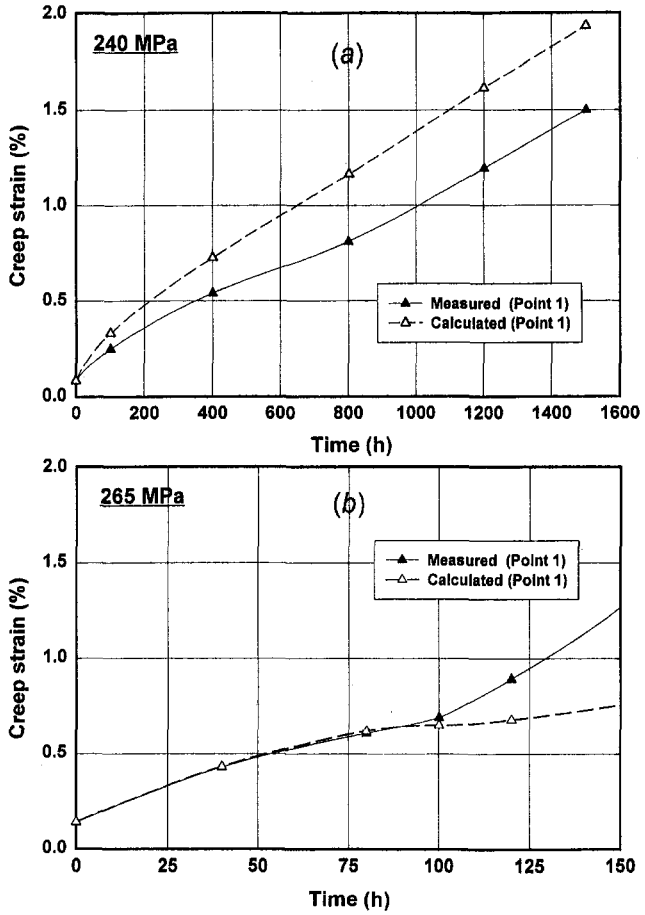

Fig. 7 Calculated and measured creep strains in the weld metal, under (*a*) 240 MPa; (*b*) 265 MPa

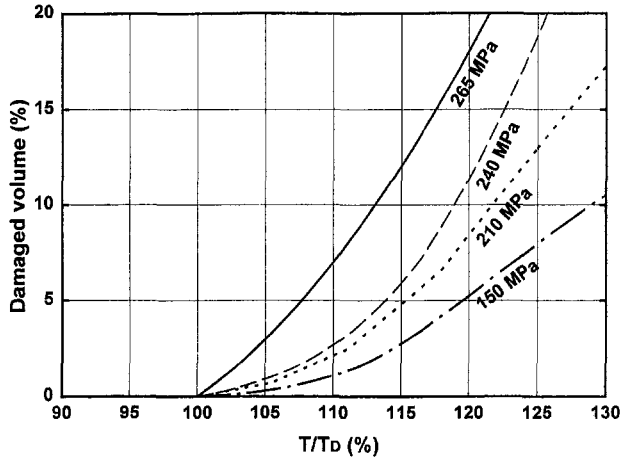

Fig. 8 Percentage of the damaged volume in the weld metal, as a function of the ratio of the current calculated time to the creep-rupture time

ratio of the current calculated time to the creep-rupture time. The plotted curves show that rupture times are evaluated with more accuracy when higher stress loadings are considered. For example, to define the rupture times to the nearest 5 percent of the damaged volume in the weldment, the uncertainty increases with small stress loading ($T/T_D \leq 107$ percent for the case of 265 MPa and $T/T_D \leq 120$ percent for the case of 150 MPa).

6 Conclusion

Tests using small as well as large full-size specimens and finite element simulations are carried out; the following conclusions are drawn:

(*a*) Feasible experiments on full-size creep specimens with real welding are demonstrated. Their results do not make it possible to observe a conclusive geometry-size effect which could exist between small and large weld thicknesses. The location of fracture for small and large joint specimens is the same and is located at the center of the weld metal. No significant difference in time to rupture is observed between these different size considerations.

(*b*) The creep laws for the base metal and for the weld metal proposed by the RCC-MR code and by Escaravage et al., respectively, are verified by the additional creep data. Some coefficient values of the weld metal creep theoretical formulas are modified in order to have a better coherence with the large full-size data.

(*c*) After having been used for the geometrical and mechanical design of the full-size specimens needed for their fabrication, finite element techniques simulating creep tests are once again performed. The calculated strains in the weld metal as well as in the base metal are in good agreement with experimental values. From the finite element results, the rupture times of the full-size specimens are predicted by considering the creep-rupture damage. Finite element stress fields show that Von Mises stresses are required in the creep-rupture damage calculation to obtain the fracture initiation in the weld metal, at the exact site as that determined by experiments. The predicted creep-rupture time are conservative and in good accord with the experimental results. The calculated evaluation of the damaged volume in the weldment shows that, concerning the time to rupture estimation, the uncertainty increases with small stress loading.

Table 5 Experimental and calculated creep-rupture times

Tests and calculations	Rupture times (h)	
	240 MPa	265 MPa
2 × Specimen 3	1964	773
2 × Specimen 4	1341	468
Full-size tests	1802	336
Finite element (model 1)	600	400
Finite element (model 2)	700	450

References

Allais, L., Dessalas, J. P., Forgeron, T., Francois, D., Huthmann, H., Escaravage, C., Poette, C., and Sassoulas, H., 1998, "Creep Behavior of Full-Size Weld Joints: Design Improvements," *Fatigue and Fracture of Engineering Materials and Structures*, Vol. 21, pp. 359–371.

ASME Code Case N47-26, 1989, "Class 1 Components in Elevated Temperature Service," ASME, New York.

CASTEM 2000, 1995, A Structural Analysis Code-User's Manual, CEA/DMT, Saclay, France.

CEC-BRITE-P2147, 1994, "Creep Behavior of Full-Size Weld Joints: Design Improvements and Defect Acceptance Criteria," CEC, Final Technical Report, RI1B-CT88-0305C.

Corum, J. M., 1990, "Evaluation of Weldment Creep and Fatigue Strength-Reduction Factors for Elevated-Temperature Design," ASME *Journal of Pressure Vessel Technology*, Vol. 112, pp. 333–339.

Dhalla, A. K., 1991, "Influence of Weld Factors on Creep Rupture Cracking at Elevated Temperature," ASME JOURNAL OF PRESSURE VESSEL TECHNOLOGY, Vol. 113, pp. 194–209.

Escaravage, C., Williamson, K., te Heesen, E., Breitling, H., Lehmann, D., and Tavassoli, A. A., 1993, "Evaluation of Mo Containing Austenitic Weld Metal Stress Rupture Strength-Factors for Use in Design," CEC, Study Contract Report, RA1-0197F.

INCA, 1986, A 2D Structural Analysis Code, CEA/DMT, Saclay, France.

Klueh, R. L., and Edmonds, D. P., 1986, "Chemical Composition Effects on the Creep of Type 316 and 16-8-2 Stainless Steel Weld Metal," *Welding Journal,* Vol. 65(6), pp. 156s–162s.

Lundqvist, B., and Anderson, T., 1982, "Creep Strength of Weld Metal and Welded Joints in Austenitic CrNi Steels and Ni Alloys," Schweissen in der Kerntechnik Aachen.

Mathew, M. D., Sasikala, G., Mannan, S. L., and Rodriguez, P., 1993, "A Comparative Study of the Creep Rupture Properties of Type 316 Stainless Steel Base and Weld Metals," ASME *Journal of Engineering Materials and Technology,* Vol. 115, pp. 163–170.

Ohrt, E., and te Heesen, E., 1991, "Optimized Materials for the Future Breeder Line," *Nuclear Engineering and Design,* Vol. 130, pp. 1–5.

Piques, R., and Pineau, A., 1984, "An Experimental Study of the Elastoplastic Behavior of Type ICL 316 SPH Stainless Steel Plate," Centre des Matériaux, ENSMP, Report G2M/12-84/RP-AP, Paris.

RCC-MR, 1993, "Design and Construction Rules for Mechanical Components of FBR Nuclear Islands," AFCEN, Paris.

Roode, F., Etienne, C. F., and van Rossum, O., 1980, "Stress and Strain Analyses for Creep and Plasticity of Welded Joints in AISI 316," International Conference on Engineering Aspects of Creep, Vol. 2, pp. 123–129, Sheffield.

Samuelson, L. A., Segle, P., and Tu, S. T., 1992, "Design of Welded Joints Subjected to High Temperature Creep," ASME PVP-Vol. 230, *Stress Classification, Robust Methods and Elevated Temperature Design,* pp. 1–6.

Senior, B. A., 1990, "Effect of Phase Transformation on the Creep Rupture Properties of Two Type 316 Weld Metals," *Journal of Materials Science,* Vol. 25, pp. 45–53.

Smith, J. J., and Farrar, R. A., 1993, "Influence of Microstructure and Composition on Mechanical Properties of Some AISI 300 Series Weld Metals," *International Materials Review,* Vol. 38, pp. 25–51.

Wood, D. S., 1985, "The Stress Rupture Properties of Austenitic Steel Weld Metals," CEC, Nuclear Science and Technology, EUR 10124 EN, Luxembourg.

Yamazaki, M., Monma, Y., Hongo, H., Watanabe, T., Kinugawa, J., and Muramatsu, Y., 1991, "Creep Rupture Behavior of Butt Welded Joint of 304 Stainless Steel Thick Plate Using Small and Large Specimens," *Transactions NRIM,* Vol. 33, pp. 64–71.